John Hubbert

Microphysical interpretation of coincident simultaneous and fast alternating horizontal and vertical polarization transmit data

J.C. Hubbert and S.M. Ellis

National Center for Atmospheric Research, Boulder CO, USA. hubbert@ucar.edu

1 September 2014

1. Introduction

The most widely used technique to achieve dual polarization measurements is by broadcasting H (horizontal) and V (vertical) polarizations simultaneously (SHV) and then receiving H and V polarization. For example, the United States National Weather Service's NEXRADs use this technique. It is well known that cross coupling of the H and V transmit waves can occur when the propagation medium is characterized by a non zero mean canting angle. This can occur in the ice phase where ice particles are aligned by an electric field (Hubbert et al. 2014a,b, 2010b; Ryzhkov and Zrnić 2007). Here experimental data from the National Center for Atmospheric Research S-band radar, S-Pol, during TiMREX (Terrain-influenced Monsoon Rainfall Experiment) are shown. The S-Pol SHV data set is complemented by FHV (fast alternating H and V transmission) data. The data are augmented with dual-Doppler and sounding data. T-matrix scattering simulations and a radar scatter model are used to explain the observed polarimetric signatures.

Small convective cells were observed to have both large positive and large negative K_{dp} (specific differential phase) values. Negative K_{dp} regions suggest that ice crystals are vertically aligned by electric fields. Since high $|K_{dp}|$ values of 0.88 deg./km in both negative and positive K_{dp} regions in the ice phase are accompanied by Z_{dr} values close to 0 dB, it is inferred that there are two types of ice crystals present: 1) smaller aligned ice crystals that cause the K_{dp} signatures and 2) larger aggregates or graupel that cause the Z_{dr} signatures. The inferences are supported with simulated ice particle scattering calculations. A radar scattering model is used to explain the anomalous radial streaks in SHV Z_{dr} and LDR.

2. S-Pol SHV and FHV Data from TiMREX

The SHV and FHV Data were gathered on 2 June 2008 in southern Taiwan at 0613:59UTC and 0619:59, respectively. An over view of the storm and data set are given in Hubbert et al. (2014a). Both data sets demonstrate the effects of cross-coupling during propagation due to aligned, canted ice particles. Figure 1 shows PPIs of FHV Z, Z_{dr}, and ϕ_{dp} in the left hand column while SHV Z, Z_{dr}, and ϕ_{dp} are given in the right column, both at both at 8.6° elevation angle. Figure 2 shows the accompanying K_{dp}^{fhv}, K_{dp}^{shv}, LDR_h (Linear Depolarization Ratio for H transmit, hereafter referred to as just LDR) and ρ_{hv}^{fhv}. LDR, Z_{dr}^{fhv}, ρ_{hv}^{fhv} clearly show the melting level at the 30 km range ring. The ρ_{hv}^{shv} is not shown since it is very similar to ρ_{hv}^{fhv}.

Bias due to cross-coupling is evidenced by the radial stripes beyond the melting level in Z_{dr}^{shv} of Fig. 1e and in LDR of Fig. 2b (Ryzhkov and Zrnić 2007; Hubbert et al. 2010b). These radial stripes are caused by aligned ice particles that have a non-zero mean canting angle. The most prominent stripes in Z_{dr}^{shv} and LDR are delineated by three dashed lines: lines (x), (y) and (z) mark the FHV data plots while lines (u), (v) and (w) mark the SHV data plots. The lines do not mark the same region in the SHV and FHV data due to storm movement between the two measurement times. The middle lines mark approximately the radial where Z_{dr}^{shv} (LDR) decrease (increase) maximally. These two striped regions are the focus of our analysis. Similar X-band data is also shown in Hubbert et al. (2014a).

Dashed line (w) for Z_{dr}^{shv} data of Fig. 1e marks the approximate right edge of the *decreasing*, biased Z_{dr}^{shv} area. This decreasing Z_{dr}^{shv} region begins at about 45 km and extends to roughly 65 km in range which corresponds to heights of 6.85 km and 9.97 km AGL, and -10°C to -35°C, respectively. Wind vector analysis of this storm is given in Hubbert et al. (2014a). Beyond 65 km Z_{dr}^{shv} remains relatively constant along the radials between lines (u) and (w). The K_{dp}^{shv} of Fig. 2 shows two small areas with negative values (minimum of $-0.8°\ \mathrm{km}^{-1}$) with the larger area located along dashed line (w) also at roughly 60 km range. The two negative K_{dp}^{shv} areas roughly correspond to the two higher reflectivity areas. We infer that a local electric field was produced by the convection in these areas which vertically aligned the smaller ice particles, thus causing the negative K_{dp}^{shv}. We also infer that since decreasing Z_{dr}^{shv} mostly

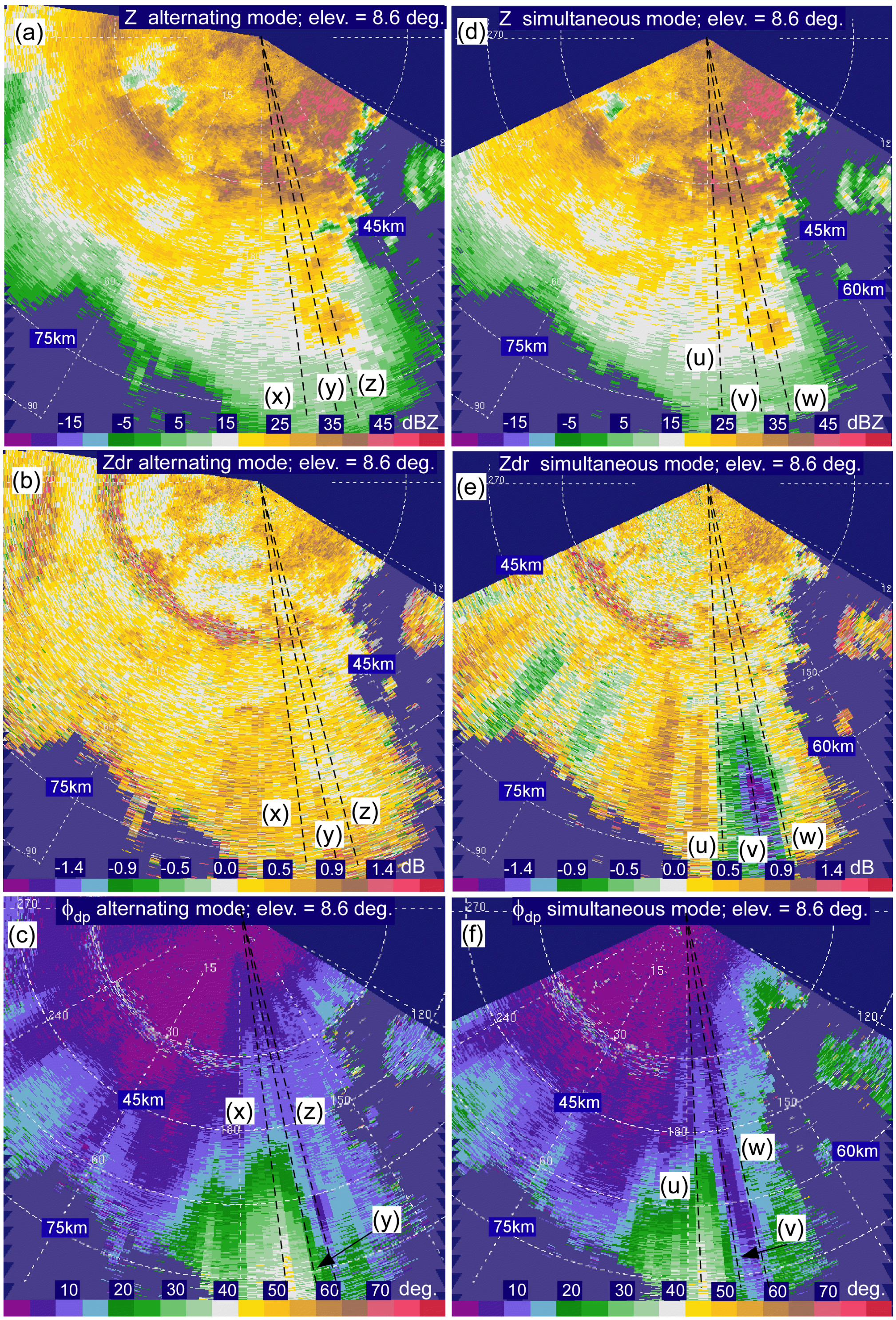

Figure 1: *S-Pol data from TiMREX. Lefthand side is FHV data while the righthand side is SHV data. The FHV and SHV data are separated by 5.5 minutes.*

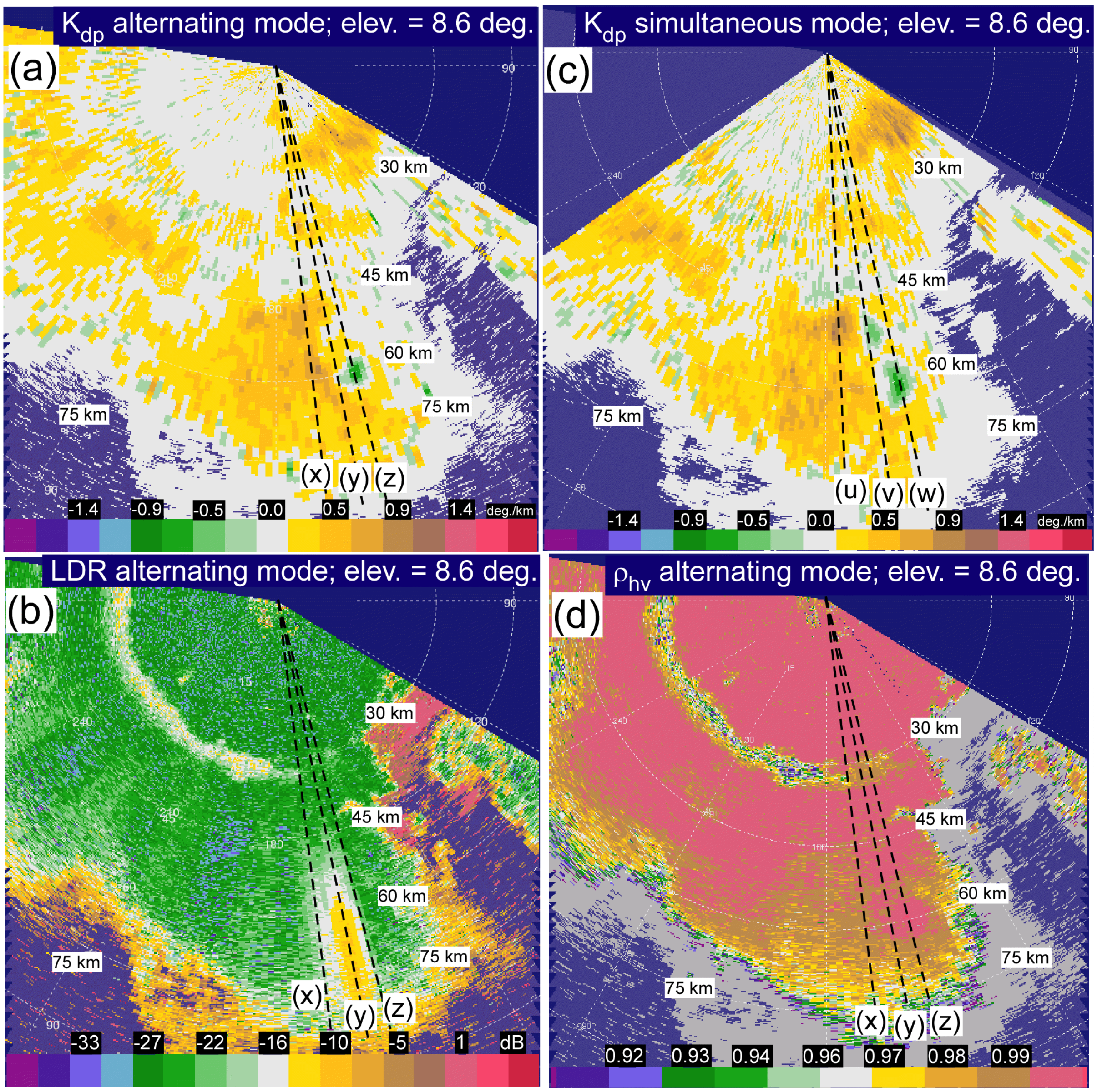

Figure 2: Data corresponding to Fig. 1: (a) K_{dp}^{fhv}, (b) LDR_h, (c) K_{dp}^{shv}, and (d) ρ_{hv}.

occurs between 45 km and 65 km, this is the region, between lines (w) and (u), where there are evidently aligned canted ice crystals causing the negative bias in Z_{dr}^{shv}.

Next examine LDR in Fig. 2b. Dashed lines (x), (y) and (z) mark the region where LDR increases from -27 dB to about -12 dB. The region is analogous to the above decreasing Z_{dr}^{shv} region: both are caused by cross-coupling due to aligned canted ice crystals and the intrinsic LDR of the canted ice crystals is masked by the LDR of the larger ice particles. For example ice columns (plates) with a axis ratio of 3 (0.33) canted at $45°$ have an LDR of about -13 (-12) dB. It is difficult to say what the LDR is for the larger ice particles since the LDR system limit of S-Pol is roughly -30 dB (Hubbert et al. 2010a). The region of the majority of the LDR increase is again roughly 45 km to 65 km. Thus, this area from 45 km to 65 km between lines (x) and (y) is analogous to the region in the SHV data from 40 km to 65 km between lines (u) and (w). The Z^{fhv} of Fig. 1a shows the two convective cores along the line (z) again at about 50 km and 60 km with peak reflectivities of about 33 dBZ. The two cores have advected to the east about 6 km during the 5.5 minute time difference between the FHV and SHV scans. The Z_{dr}^{fhv} can be considered as a much more accurate estimate of the intrinsic Z_{dr} in this region than Z_{dr}^{shv} since the effects of cross-coupling are negligible on Z_{dr}^{fhv} (Wang and Chandrasekar 2006). In the region of increasing LDR between lines (y) and (z), Z_{dr}^{fhv} is slightly positive on average. To the west between lines (x) and (y), Z_{dr}^{fhv} is a bit more positive, especially along line (x) where Z_{dr}^{fhv} is around 0.4 dB. In the next 15 km farther west beyond line (x) in the ice phase, Z_{dr}^{fhv} is between 0.4 dB and 1 dB, and K_{dp} is 0.3 to $0.8°$ km^{-1} most everywhere.

a. *Negative* $\mathbf{K_{dp}}$

Corresponding to the higher reflectivities along lines (z) and (w) are areas of negative K_{dp} marked in green color scale in both the SHV and the FHV data of Fig. 2a,c. The peak negative K_{dp} is approximately $-0.8°$km^{-1} for both the SHV and FHV data. This is a relatively large value in the ice phase and indicates that there is a significant population of ice particles with their major axis oriented near vertical and with large major to minor axis ratios. Examining the Z_{dr}^{fhv}, it is seen that the intrinsic Z_{dr} in these regions is close to 0 dB. Simulations discussed below show that ice crystals that produce a K_{dp} of $-0.8°$km^{-1} would also produce significantly negative Z_{dr}, smaller than -3 dB. Thus, in these regions there are likely two ice crystal population types 1) a high concentration of near vertically aligned small ice crystals with a high axis ratio, resulting in negative K_{dp}, and 2) larger ice particles that are randomly oriented and dominate the backscatter signature, thus producing a near zero Z_{dr}. Kennedy and Rutledge (2011) have modeled oriented dendrites in winter storms over the Front Range of Colorado with larger aggregates that masked the higher Z_{dr} of the dendrites. Recently, Andrić et al. (2013) also compiled scattering calculations for vertical profiles of polarimetric radar data using different types of ice particles for a winter storm in Oklahoma. Their model, however, was unable to predict their higher observed K_{dp}. The radar data and dual-Doppler analysis above indicate that weak convection was taking place (vertical velocities of 2 to 6 m s^{-1}) so that that ice crystals (columns and plates) were being produced (Bailey and Hallett 2009). It is very likely that electrification was occurring which aligned the ice crystals.

Moving west of lines (z) and (w), the amount of cross-coupling increases, as is evidenced in the Z_{dr}^{shv} and LDR plots (Figs. 1e and 2b), until lines (y) and (v) which mark the radials of near maximum cross-coupling. Lines (y) and (v) also approximately mark the transition area between the negative K_{dp} and positive K_{dp} areas. Moving further to the west to lines (x) and (u), the amount of cross-coupling decreases while K_{dp} increases. These lines also mark the radials of maximum ϕ_{dp} accumulation as seen Fig. 1c,f. Reflectivities also decrease to 15-20 dBZ. The K_{dp} is high with a maximum of $1°$km^{-1}; however, Z_{dr}^{fhv} is only slightly positive around 0.5 dB on average. Again, this indicates that there are two ice crystal population types: 1) smaller, near horizontally aligned ice crystals that give high K_{dp} and 2) larger randomly oriented particles that mask the high Z_{dr} of the horizontally aligned crystals.

Summarizing, the polarimetric signatures indicate that along lines (z) and (w) there are vertically aligned ice crystals mixed with larger aggregates or graupel. The vertical alignment is very likely due to the presence of electric fields. Moving to the west, the electric field gives ice particles a mean canting angle of around $45°$ along lines (y) and (v) where cross coupling is maximized (Hubbert et al. 2014a). Moving farther west where there is apparent weak electric fields so that vertical alignment does not occur, the ice crystals are horizontally aligned likely by aerodynamic forcing along lines (x) and (u) where K_{dp} becomes quite positive, maximum ϕ_{dp} accumulation occurs and the cross-coupling is greatly reduced. Moving even father west additional radial streaks in Z_{dr}^{shv} and in LDR are seen indicating that the ice crystals obtain mean canting angles significantly away from $0°$ so that cross-coupling again occurs. However, the mean canting angle does not exceed $\pm 45°$ since K_{dp} remains positive (Hubbert et al. 2014a; Ryzhkov and Zrnić 2007). The observed negative K_{dp} at the far southern edge of the storm are due to low SNR and are artifacts of the K_{dp} algorithm rather than microphysics. Z_{dr}^{fhv} remains around 0 dB or slightly positive through the western region

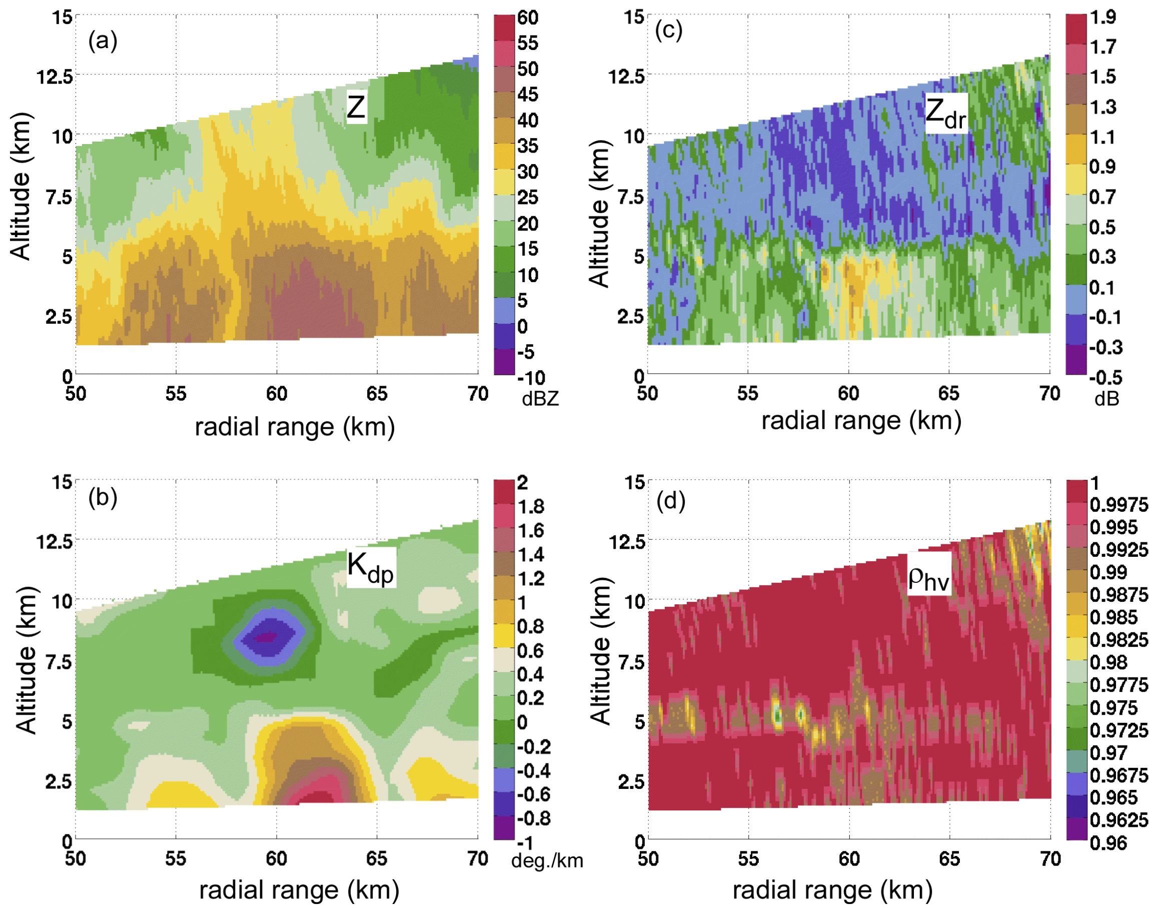

Figure 3: *Vertical FHV data cross sections along line (z) of Fig. 2a that illustrates the negative K_{dp}^{fhv} region.*

where K_{dp} is quite positive (0.3 to $0.8°\mathrm{km}^{-1}$) again indicating the coexistence of two populations of ice particle types as discussed above.

To illustrate the vertical structure of the negative K_{dp} and the accompanying radar signatures, Fig. 3 shows a radial vertical cross section of FHV Z, Z_{dr}, K_{dp} and ρ_{hv}, as labeled, along line (z) of Fig. 2a. In the area of negative K_{dp}, Z_{dr}^{fhv} is -0.1 to -0.3 dB, Z^{fhv} is 25 to 35 dBZ, and ρ_{hv}^{fhv} is quite high indicating good data quality. Negative K_{dp} such as seen in Fig. 2a,c are fairly common in TiMREX data. Figure 4 show three more examples of negative K_{dp}. All of these three cases are associated with shallow convective cores (there are several more cases not shown here). The reflectivities are in the 23 dBZ to 35 dBZ range, Z_{dr} is close to zero, ρ_{hv} is high (> 0.98) and typically, radial LDR streaks are associated indicating canted ice particles are causing cross-coupling. Thus, electric fields are likely present in these regions.

3. Discussion and Conclusions

In this paper, cross coupling of simultaneously transmitted H and V waves, due to canted ice crystals, was presented, simulated, and analyzed. Microphysical interpretations were offered. Both SHV and FHV S-Pol data from TiMREX were examined in detail. The analyzed SHV data and FHV data were gathered within 5.5 min of each other in a convective storm complex so that polarimetric signatures could be compared. Cross coupling in the ice phase was evident from radial steaks in Z_{dr}^{shv} and LDR. Three regions surrounding the cross-coupling signatures were examined and micophysically interpreted: 1) an area with negative K_{dp}, Z_{dr} of about 0dB, and high reflectivity; 2) an area with small K_{dp}, near-zero Z_{dr} maximum cross coupling, and somewhat smaller reflectivity; and 3) an area with high positive K_{dp}, small positive Z_{dr} (about 0.5dB on average), maximum ϕ_{dp} accumulation, and small cross coupling. All

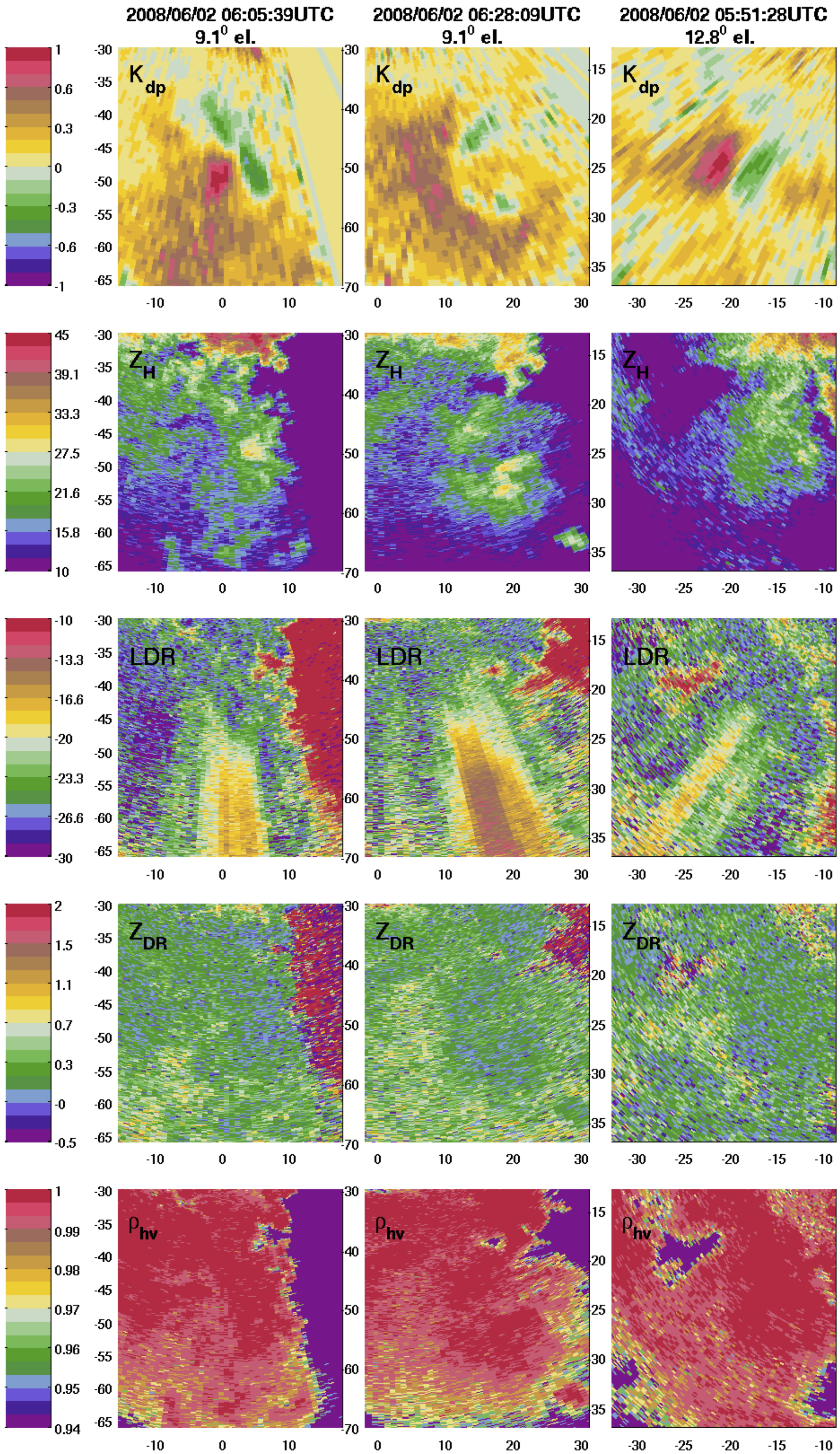

Figure 4: *Three examples of negative K_{dp} with accompanying Z_H, LDR Z_{dr} and ρ_{hv}.*

three areas can be characterized by two distinct populations of ice particles: 1) smaller aligned ice crystals (columns or plates) with large major to minor axis ratios that cause large K_{dp} with relatively small reflectivity and 2) larger randomly oriented ice particles with larger reflectivity that mask the $Z_{dr}$of the smaller aligned ice crystals. Sounding data and dual-Doppler analysis showed that moderate updrafts of $26\,\mathrm{ms}^{-1}$ were present in a humid environment and likely resulted in supersaturated conditions (with respect to ice), supercooled liquid water, and rimed particles in the convective updrafts (Hubbert et al. 2014a). Because of the observed negative K_{dp} (minima of $-0.8°\mathrm{km}^{-1}$), an electric field was likely present that aligned the columns or plates of high axis ratio and high density. Since the reflectivity was high in this region and $Z_{dr}$was close to 0 dB, larger graupel particles were likely present. The presence of ice crystals with graupel and supercooled liquid in an updraft are conditions conducive for charge separation. The negative K_{dp} was observed at other times and in other storms of similar composition and character: moderate storm depth with likely moderate updrafts, high reflectivities in ice, 610 km AGL, high ρ_{hv}, and near-zero Z_{dr}. Both LDR streaks and high K_{dp} areas are typically associated with the negative K_{dp} areas as was illustrated in three cases in Fig. 4. The ensuing electric field could further accelerate ice crystal growth and possible fragmentation so that there is an abundance of small crystals with high axis ratios that are able to cause the observed high K_{dp}.

Acknowledgment

This research was supported in part by the ROC (Radar Operations Center) of Norman OK. The NCAR S-Pol radar is supported by the National Science Foundation. Any opinions, findings and conclusions or recommendations expressed in this publication are those of the authors and do not necessarily reflect the views of the National Science Foundation.

References

Andrić, J., M. Kumajian, D. Zrnić, J. Straka, and V. Melnikov, 2013: Polarimetric signatures above the melting layer in winter storms: An observational and modeling study. *J. Appl. Meteor. Climat.*, **52**, 682–700.

Bailey, M. and J. Hallett, 2009: A comprehensive habit diagram for atmospheric ice crystals: Confirmation from the laboratory, AIRS II and other field studies. *J. Atmos. Sci.*, **66**, 2888–2899.

Hubbert, J., S. Ellis, W.-Y. Chang, M. Dixon, and Y.-C. Liou, 2014a: X-band polarimetric observations of cross-coupling in the ice phase of convective storms in taiwan. *J. of Applied Meteor. and Clim.*.

Hubbert, J., S. Ellis, W.-Y. Chang, S. Rutledge, and M. Dixon, 2014b: Microphysical interpretation of S-band simultaneous horizontal and vertical polarization transmit radar data. *J. of Applied Meteor.and Clim.*.

Hubbert, J., S. Ellis, M. Dixon, and G. Meymaris, 2010a: Modeling, error analysis and evaluation of dual polarization variables obtained from simultaneous horizontal and vertical polarization transmit radar. Part I: Modeling and antenna errors. *J. Atmos. Oceanic Technol.*, **27**, 1583–1598.

— 2010b: Modeling, error analysis and evaluation of dual polarization variables obtained from simultaneous horizontal and vertical polarization transmit radar. Part II: Experimental data. *J. Atmos. Oceanic Technol.*, **27**, 1599–1607.

Kennedy, P. C. and S. A. Rutledge, 2011: S-band dual-polarization radar observations of winter storms. *J. Appl. Meteor.*, **50**, 844–858.

Ryzhkov, A. and D. Zrnić, 2007: Depolarization in ice crystals and its effect on radar polarimetric measurements. *J. Atmos. Oceanic Tech.*, **24**, 1256–1267.

Wang, Y. and V. Chandrasekar, 2006: Polarization isolation requirements for linear dual-polarization weather radar in simultaneous transmission mode of operation. *IEEE Trans. Geosc. and Remote Sen.*, **44**, 2019–2028.